

Relative sea-level rise around East Antarctica during Oligocene glaciation

Paolo Stocchi^{1*†}, Carlota Escutia², Alexander J. P. Houben^{3,4}, Bert L. A. Vermeersen^{1†}, Peter K. Bijl³, Henk Brinkhuis^{1,3}, Robert M. DeConto⁵, Simone Galeotti⁶, Sandra Passchier⁷, David Pollard⁸ and IODP Expedition 318 scientists[‡]

During the middle and late Eocene (~48–34 Myr ago), the Earth's climate cooled^{1,2} and an ice sheet built up on Antarctica. The stepwise expansion of ice on Antarctica^{3,4} induced crustal deformation and gravitational perturbations around the continent. Close to the ice sheet, sea level rose^{5,6} despite an overall reduction in the mass of the ocean caused by the transfer of water to the ice sheet. Here we identify the crustal response to ice-sheet growth by forcing a glacial-hydro isostatic adjustment model⁷ with an Antarctic ice-sheet model. We find that the shelf areas around East Antarctica first shoaled as upper mantle material upwelled and a peripheral forebulge developed. The inner shelf subsequently subsided as lithosphere flexure extended outwards from the ice-sheet margins. Consequently the coasts experienced a progressive relative sea-level rise. Our analysis of sediment cores from the vicinity of the Antarctic ice sheet are in agreement with the spatial patterns of relative sea-level change indicated by our simulations. Our results are consistent with the suggestion⁸ that near-field processes such as local sea-level change influence the equilibrium state obtained by an ice-sheet grounding line.

Antarctic glaciation was abruptly established during the Eocene–Oligocene transition (EOT) in two ~200-kyr-spaced phases between 34.0 Myr and 33.5 Myr ago, as recorded by the oxygen isotope composition of marine biogenic calcite^{3,4,9} ($\delta^{18}\text{O}$). The first shift (EOT-1) is believed to represent a transient glaciation^{10–12}, later followed by the establishment of a continental-scale ice sheet across the Oligocene isotope event-1 (Oi-1, 33.7 Myr ago; ref. 4). This is consistent with Northern Hemisphere ocean-sediment cores, which indicate a 60 ± 20 m relative sea level (rsl) fall across the EOT (refs 13–15). Under isostatic equilibrium conditions, the observed regression nearly corresponds to the rsl drop expected from glacioeustasy⁶. Along the Antarctic margins, however, the rsl changes accompanying the glaciation are expected to strongly deviate from the eustatic, because of large crustal and gravitational perturbations induced by the ice sheet on the deformable Earth⁶. Furthermore, strong regional rsl change gradients would be maintained long after the ice-sheet stabilization, by the flexure

of lithosphere¹⁶. This necessitates self-consistent physical models for rsl change to compare near-field sedimentary sequences with far-field ice-sheet volume estimates.

Here we evaluate the regionally varying rsl changes in response to glacial expansion and their effects on glaciomarine facies¹⁷ around East Antarctica with a numerical model for glacial-hydro isostatic adjustment (GIA). Our model is based on the solution of the gravitationally self-consistent sea-level equation^{7,8} for a prescribed Antarctic ice-sheet chronology¹⁸ and a linear viscoelastic rheology for the solid Earth (Methods and Supplementary Information). We compare the model results with sedimentary records from the Wilkes Land Margin (Fig. 1a), recently recovered during Integrated Ocean Drilling Program (IODP) Expedition 318 (Sites U1356 and U1360; ref. 19), the Ross Sea (Cape Roberts Project; CRP-3 Core; refs 20,21) and Prydz Bay (Ocean Drilling Program (ODP) Sites 739 and 1166; refs 22,23).

The ice-sheet model employed in our GIA computations is characterized by a 2.2 Myr growth phase caused by a combination of decreasing CO_2 and orbital forcing that drives summer temperatures below the threshold for glaciation¹⁸ but uses a new reconstruction of Antarctic topography²⁴ at EOT time (Methods). The ice-sheet volume at the glacial maximum corresponds to ~69.0 m of equivalent sea level in this model, ~14.0 m more than previous modelling results¹⁸, probably owing to larger Antarctic land surface²⁴.

We run a reference simulation (Fig. 1a–d) for an Earth model defined by an elastic lithosphere thickness (LT) of 100 km, and by a viscosity profile (RVP) that is discretized into a lower mantle (LM), a transition zone (TZ) and an upper mantle (UM) and is characterized by viscosities of 1.0×10^{22} , 5.0×10^{20} and 2.5×10^{20} Pa s respectively (RVP-100 km-LT simulation). To evaluate how the GIA signal varies according to the mantle viscosity, we perform simulations for an ensemble of viscosity profiles (EVPs) characterized by viscosities varying in the range of 10^{21} – 10^{23} , 10^{20} – 10^{21} and 10^{19} – 10^{21} Pa s, respectively for LM, TZ and UM (EVP-100 km-LT simulations). We also investigate the role of the LT by comparing a thinner (60 km, upper limit for the West Antarctic Rift System) and a thicker scenario (250 km, upper limit for the East Antarctic Craton; Supplementary Information), both

¹NIOZ Royal Netherlands Institute for Sea Research, PO Box 59, 1790 AB Den Burg, Texel, The Netherlands, ²Instituto Andaluz de Ciencias de la Tierra, CSIC-UGR, 18100 Armilla, Spain, ³Department of Earth Sciences, Faculty of Sciences, Utrecht University, Budapestlaan 4, 3584 CD Utrecht, The Netherlands, ⁴Netherlands Organization for Applied Scientific Research (TNO), Princetonlaan 6, 3584 CB Utrecht, The Netherlands, ⁵Department of Geosciences, University of Massachusetts, Amherst, Massachusetts 01003, USA, ⁶Dipartimento Geo TeCA, Università degli Studi di Urbino 'Carlo Bo', Località Crocicchia, 61029 Urbino, Italy, ⁷Department of Earth and Environmental Studies, Montclair State University, Montclair, New Jersey 07043, USA, ⁸Earth and Environmental Systems Institute, Pennsylvania State University, University Park, 16802 Pennsylvania, USA, [†]Present addresses: IMAU Institute for Marine and Atmospheric Research, Utrecht University, Princetonplein 5, 3584 CC Utrecht, The Netherlands (P.S.); TU Delft Climate Institute, Astrodynamics and Space Missions, Faculty of Aerospace Engineering, TU Delft, 2629 HS Delft, The Netherlands (B.L.A.V.). [‡]A full list of IODP Expedition 318 scientists and their affiliations appears at the end of the paper. *e-mail: Paolo.Stocchi@nioz.nl

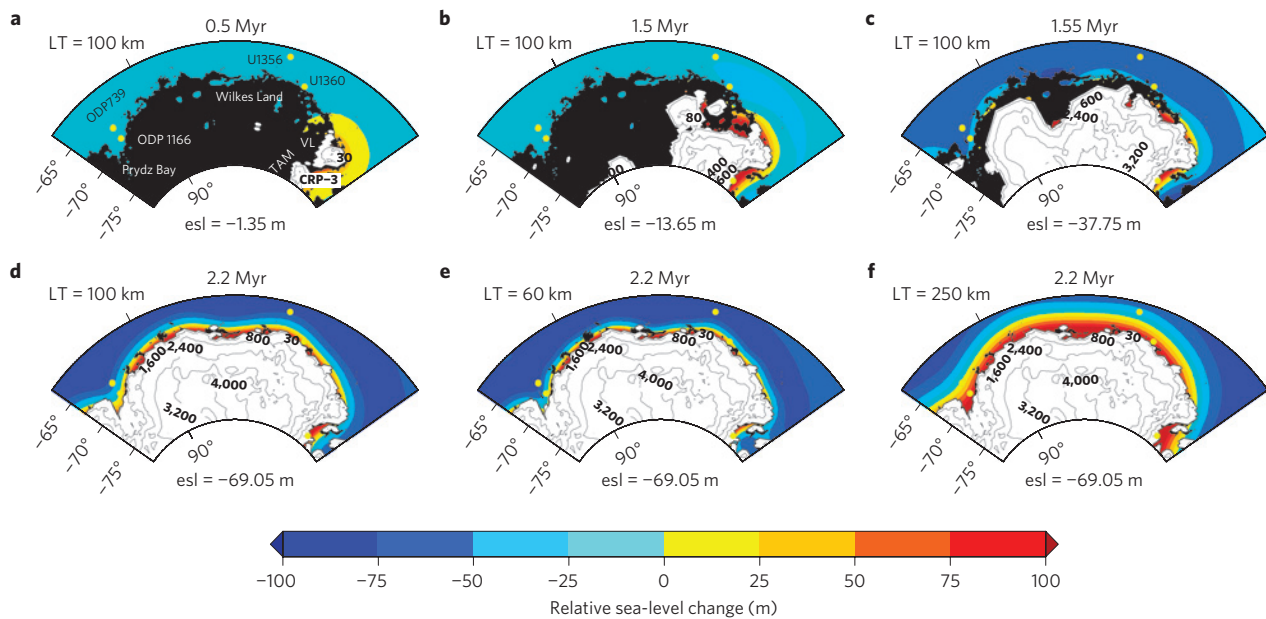


Figure 1 | East Antarctic ice-sheet evolution and rsl changes at four model run times and relative to the pre-glacial state. The ice-sheet extent is shown in white and subaerially exposed land is shown in black. The eustatic values (m) are reported as *esl*. **a–d**, Rsl model predictions according to RVP-100 km-LT. **a**, Model run time is 0.5 Myr. TAM, Trans-Antarctic Mountains; VL, Victoria Land. **b**, Model run time is 1.5 Myr. **c**, Model run time is 1.55 Myr, which correlates to the end of the first $\delta^{18}\text{O}$ step^{3,4,15}. **d**, Model run time is 2.2 Myr. **e**, Rsl change at 2.2 Myr for RVP-60 km-LT. **f**, Rsl change at 2.2 Myr for RVP-250 km-LT.

combined to RVP (RVP-60 km-LT and RVP-250 km-LT). A 175 km LT is also considered for Prydz Bay.

RVP-100 km-LT shows that by 0.5 Myr (model run time), when ~ 1.5 m of equivalent sea level is stored in ice caps over the Trans-Antarctic Mountains and northern Victoria Land, the surrounding continental shelves already experience a noticeable ice-induced rsl rise (~ 50.0 m rsl rise at Site CRP-3 in the Ross Sea; Fig. 1a). Further offshore and westwards, a peripheral uplifting forebulge generated by the upwelling of upper mantle material contributes to a rsl drop that is comparable to or slightly larger than the eustatic. This spatial pattern of rsl change is maintained during the growth and coalescence of the ice caps (Fig. 1b). By 1.55 Myr (Fig. 1c), the first rapid pulse of continental-scale glaciation results in vertical and lateral expansion of the peripheral forebulge. At the distal Sites U1356 (Wilkes Land Margin) and 739 (Prydz Bay), the model simulation predicts rsl drops that are ~ 25.0 m and ~ 32.0 m larger than the eustatic, respectively (Fig. 1c). Now, the areas of subsidence narrow towards the coastlines. By 2.2 Myr, the proximal Sites U1360 (Wilkes Land) and 1166 (Prydz Bay) experience ice-induced crustal subsidence and are respectively ~ 42.0 and ~ 7.0 m deeper than before the onset of glaciation (Fig. 1d). The latitudinal extent of the subsiding area strongly depends on the lithosphere thickness (Fig. 1d–f): for a 60-km-thick lithosphere, subsidence is confined between the inner shelf and the coast (Fig. 1e), whereas the flexure of 250-km-thick lithosphere enhances rsl rise offshore (Fig. 1f).

On the Wilkes Land shelf (Site U1360) the RVP-100 km-LT and EVP-100 km-LT simulations show that the first two pulses of glacial expansion (1.50–1.70 Myr) are accompanied by a rsl drop larger than the eustatic case (Fig. 2a). After ~ 1.70 Myr, a rapid 75–100 m rsl rise re-establishes, or even exceeds, the initial depth by ~ 50.0 m. This pronounced increase in rsl is due to the nearby grounding and thickening of ice that depresses the lithosphere and gravitationally attracts ocean water. By 2.2 Myr, the site is 40–60 m deeper than at the beginning. The same is obtained for RVP-60 km-LT, whereas no regressive phase is predicted for RVP-250 km-LT, and this simulation yields a final ~ 80.0 m rsl rise. For 60- and 100-km-thick lithosphere, the distal Site U1356 experiences a rsl drop that is

20–30 m larger than the eustatic until ~ 1.70 Myr, and is later followed by an almost steady rsl. For RVP-250 km-LT, the rsl drop is initially larger than the eustatic until ~ 1.60 Myr, then stays close to the eustatic until ~ 1.70 Myr, and is later followed by a sudden ~ 20 m rise that, in contrast to the U1360 case, does not reach the initial position. The succession recovered at shelf Site U1360 consists of clast-bearing, glacially influenced sediments of which the base correlates to the Oi-1 (ref. 19; Fig. 3a and Supplementary Information). This overlies the regionally widely recognized unconformity WLU3, which represents a regressive or even an amalgamated regressive–transgressive surface²⁵ (Supplementary Information). The Oligocene strata are consistent with a glaciomarine shelf environment with a fining-upward sedimentary sequence¹⁹ that can be a consequence of subsidence imposed by either remote ice melting or close ice thickening. All of our simulations support the latter. Only model results based on 100- or 60-km-thick lithosphere are able to explain the initial regressive phase inferred from seismic data, suggesting that a 250-km-thick lithosphere may be too thick for Wilkes Land Subglacial Basins.

The base of the Oligocene succession at the distal Site U1356 overlies a major (12 Myr) hiatus¹⁹ separating it from middle Eocene (>46 Myr old) strata (Supplementary Information). This is remarkable because the Australo-Antarctic Gulf underwent a long-term tectonic deepening²⁶. The oceanographic consequences of accelerated deepening of the Tasman Gateway in the late Eocene²⁷ may have partially contributed to the removal of sediments. However, a direct contribution to the hiatus is expected from the seafloor deformation associated with ice-sheet loading. In fact, deposition started by the end of the erosional phase and is in close correspondence with the stabilization of the bathymetry at the Oi-1. This overall pattern is in agreement with the stable rsl predicted by the GIA models after ~ 1.8 Myr.

At Site CRP-3 (Ross Sea), the first pulse of continental-scale glaciation occurring at ~ 1.5 Myr results in a regional uplift. This ends the local long-term trend of rsl rise that is caused by the nearby ice caps (Transantarctic Mountains and northern Victoria Land) and shared by all of the simulations (Fig. 2c). A sudden 40–60 m rsl

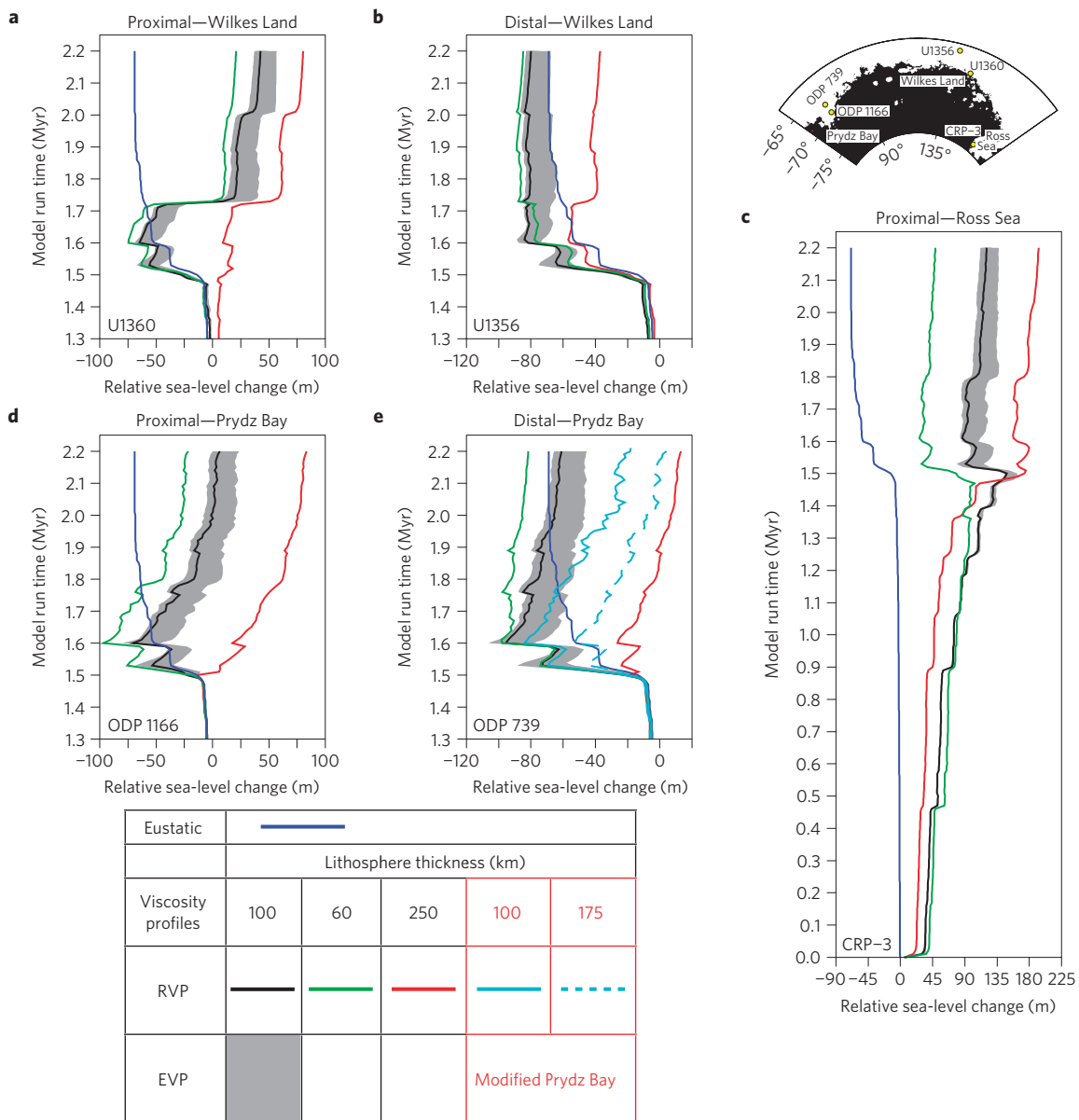


Figure 2 | Rsl predictions at the sites considered in this study according to different Earth models and relative to the pre-glacial state. The rsl change is shown as a function of model run time. **a–e**, The blue curve refers to the eustatic sea-level change and shows two main pulses, respectively, at ~1.5 Myr and ~1.6 Myr; the black rsl curve refers to the RVP-100 km-LT simulation; the green rsl curve refers to the RVP-60 km-LT simulation; the red rsl curve refers to the RVP-250 km-LT simulation; the dark grey band refers to EVP-100 km-LT simulations. **a**, Wilkes Land, IODP Site U1360. **b**, Wilkes Land, IODP Site U1356. **c**, Ross Sea, Cape Roberts CRP-3. **d**, Prydz Bay, ODP Site 1166. **e**, Prydz Bay, ODP Site 739. Here the effects of an extended ice sheet on the continental shelf are included. The solid cyan curve refers to RVP-100 km-LT simulation; the dashed cyan curve refers to RVP-175 km-LT case (modified Prydz Bay; see Supplementary Information).

drop is obtained according to the 60- and 100-km-thick lithosphere cases; a slowing of the rsl change is predicted for RVP-250 km-LT. According to all of the simulations, a moderate rsl rise, punctuated by short-term fluctuations, follows from ~1.6 Myr onwards. The overall predicted rsl trends are supported by the observed transition from a fluvial to a shelfal depositional setting above the storm wave base in the lower part of the CRP-3 core (Fig. 3b and Supplementary Information). The progressively decreasing frequency of clast abundance maxima, accompanied by an increasing proportion of sand, depicts a longer-term transgression that, on the basis of the available stratigraphic models²¹, culminates at the Oi-1 (Fig. 3b). Later, a transition to an inner-shelf depositional setting above the fair-weather wave base occurs (Supplementary Information). Above the Oi-1 level, a longer-term regression trend, indicated by

the progressively increasing frequency of clast abundance peaks, culminates at ~400 metres below sea floor (mbsf), with the transition to a pro-deltaic sedimentary environment²¹. On the basis of the sedimentary succession of Site CRP-3 we infer a long-term transgression and subsequent regression across the EOT. These trends reflect rsl changes not larger than ~20.0 m (Fig. 3b and Supplementary Information). However, on correction for sediment accumulation, the different rates of increase in accommodation space before and after Oi-1 suggest that the EOT rsl rise was of the order of 70–80 m (Supplementary Information), therefore in agreement with RVP- and EVP-100 km-LT.

At Prydz Bay Sites, the modelling results are broadly consistent with those for Wilkes Land. Simulations according to 60 and 100 km LT cases show that a regressive phase ends at ~1.6 Myr with the

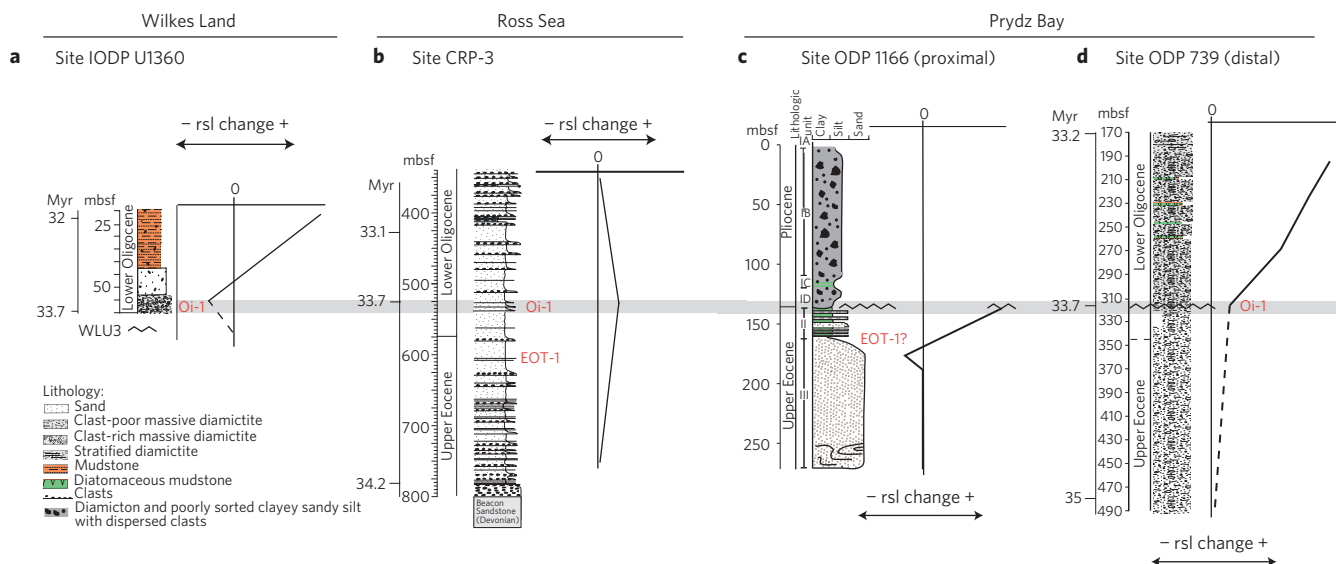


Figure 3 | Sedimentary records considered in this study and inferred qualitative rsl changes. a, Wilkes Land, IODP Site U1360. **b**, Ross Sea, Cape Roberts CRP-3. **c**, Prydz Bay, ODP Site 1166. **d**, Prydz Bay, ODP Site 739.

arrival of the ice sheet at the coast, and is followed by rsl rise (Fig. 2d–e). As for U1360, the initial regression is not predicted according to RVP-250 km-LT. The Oi-1 level (at 319 mbsf) at Site 739 corresponds landward with a regional unconformity that can be traced south to Site 1166 (Fig. 3c). This unconformity onlaps landward, indicating an increase in accommodation space²⁸. We postulate that the ice sheet advanced beyond the location of Site 1166, but did not cover Site 739 (ref. 29). The ice-sheet model is altered to test this hypothesis and, combined with RVP-100 km-LT and/or RVP-175 km-LT, provides a ~40.0 m larger rsl rise at Site 739 (cyan curves in Fig. 2e). This result further supports the expanded marine lower Oligocene succession at Site 739 (Fig. 3d).

The observed occurrence of rsl rise across the Oi-1 along the East Antarctic margins is apparently at odds with the 60 ± 20 m glacio-eustatic sea-level drop as inferred from the Northern Hemisphere geological records. A solution to this conundrum is found when accounting for ice-load-induced solid Earth deformations and gravitational perturbations in the interpretation of the near-field rsl changes. As the volume of our new Antarctic ice-sheet model (~70 m esl) matches with the middle to upper value of the inferred Northern Hemisphere rsl drop, the formal inclusion of GIA-driven perturbations reconciles the Northern Hemisphere regression with the near-field formation of accommodation space for sediments throughout the Oi-1. The associated infill of sediments is expected to further alter the rsl change along the Antarctic margins, and should therefore be included in a gravitationally self-consistent manner within the GIA models. These models are here mostly sensitive to the lithosphere thickness. Furthermore, the large rsl rise in the proximity of the Antarctic ice-sheet margins might provide a strong dynamical feedback to the ice-sheet stability, which is theoretically in line with the revised version of Weertman's law⁸.

Methods

To simulate the changes accompanying the Antarctic ice-sheet growth, we solve the gravitationally self-consistent sea-level equation using the pseudo-spectral method and accounting for coastline migration and grounding/floating of marine ice^{7,16}. We employ a spherical, self-gravitating, viscoelastic, irrotational, incompressible and radially stratified Earth model (Supplementary Information). We implement an ice-sheet chronology simulated by an offline hybrid ice-sheet/shelf model³⁰ run at 40 km resolution. The ice model is driven by an interpolated matrix of global climate model climatologies³⁰, accounting for gradually decreasing CO₂ (from $\times 6$ to $\times 2$ pre-industrial levels over a 2-Myr interval) across the EOT. Oceanic melt rates under ice shelves assume a relatively warm ocean appropriate for the early

Oligocene, and are the same as those used to represent the warm Pliocene in ref. 30. The 2-Myr period of simulated ice-sheet growth is discretized into 10-kyr time steps. Solid Earth boundary conditions are provided by a new palaeotopographic reconstruction of Antarctica at 34 Myr (ref. 24) with a mostly subaerial West Antarctica. Basal sliding coefficients assume hard bedrock where ice-free elevations are above sea level. Simulated ice volume is ~69.0 m of equivalent sea level (esl), ~14.0 m larger than in previous modelling results⁸ and in closer agreement with estimates of EOT rsl fall interpreted from Northern Hemisphere shallow marine sections^{13–15}. The new Antarctic topography²⁴ is used from 90° S to 61° S as part of the initial (undeformed) global land/ocean mask in the GIA model. North of 61° S, the Antarctic reconstruction is merged with a standard global tectonic reconstruction (Supplementary Information).

Received 6 August 2012; accepted 28 February 2013;
published online 21 April 2013

References

- Zachos, J. C., Dickens, G. R. & Zeebe, R. E. An early Cenozoic perspective on greenhouse warming and carbon-cycle dynamics. *Nature* **451**, 279–283 (2008).
- Liu, Z. *et al.* Global cooling during the Eocene–Oligocene climate transition. *Science* **323**, 1187–1190 (2009).
- Coxall, H. K. & Wilson, P. A. Early Oligocene glaciation and productivity in the eastern equatorial Pacific: Insights into global carbon cycling. *Palaeoceanography* **26**, PA2221 (2011).
- Scher, H. D., Bohaty, S. M., Zachos, J. C. & Delaney, M. L. Two-stepping into the icehouse: East Antarctic weathering during progressive ice-sheet expansion at the Eocene–Oligocene transition. *Geology* **39**, 383–386 (2011).
- Woodward, R. S. On the form and position of mean sea level. *United States Geol. Surv. Bull.* **48**, 87–170 (1888).
- Raymo, M. E. *et al.* Departures from eustasy in Pliocene sea-level records. *Nature Geosci.* **4**, 328–332 (2011).
- Kendall, R. *et al.* On post-glacial sea level – II. Numerical formulation and comparative results on spherically symmetric models. *Geophys. J. Int.* **154**, 253–267 (2003).
- Gomez, N. *et al.* Evolution of a coupled marine ice sheet-sea level model. *J. Geophys. Res.* **117**, F01013 (2012).
- Zachos, J. C., Quinn, T. M. & Salamy, K. A. High-resolution (10⁴ years) deep-sea foraminiferal stable isotope records of the Eocene–Oligocene climate transition. *Palaeoceanography* **11**, 251–266 (1996).
- Lear, C. H., Bailey, T. R., Pearson, P. N., Coxall, H. K. & Rosenthal, Y. Cooling and ice growth across the Eocene–Oligocene transition. *Geology* **36**, 251–254 (2008).
- Wade, B. S. *et al.* Multiproxy record of abrupt sea-surface cooling across the Eocene–Oligocene transition in the Gulf of Mexico. *Geology* **40**, 251–254 (2008).
- Bohaty, S. M., Delaney, M. L. & Zachos, J. C. Foraminiferal Mg/Ca Evidence for Southern Ocean Cooling across the Eocene–Oligocene Transition. *Earth Planet. Sci. Lett.* **317–318**, 251–261 (2012).
- Kominz, M. A. & Pekar, S. F. Oligocene eustasy from two-dimensional sequence stratigraphic backstripping. *GSA Bull.* **113**, 291–304 (2001).

14. Miller, K. G. *et al.* Eocene–Oligocene global climate and sea-level changes: St. Stephens Quarry, Alabama. *GSA Bull.* **120**, 34–53 (2008).
15. Houben, A. J. P. *et al.* The Eocene–Oligocene transition: Changes in sea level, temperature or both? *Palaeogeogr. Palaeoclimatol. Palaeoecol.* **335–336**, 75–83 (2012).
16. Gomez, N. *et al.* A new projection of sea level change in response to collapse of marine sectors of the Antarctic Ice-Sheet. *Geophys. J. Int.* **180**, 623–634 (2010).
17. Boulton, G. S. in *Glaciomarine Environments. Processes and Sediments* Vol. 53 (eds Dowdeswell, J. A. & Scourse, J. D.) 15–52 (Geological Society of London, Special Publications, 1990).
18. DeConto, R. & Pollard, D. Rapid Cenozoic Antarctic glaciation of Antarctica induced by declining atmospheric CO₂. *Nature* **421**, 245–249 (2003).
19. Escutia, C. *et al.* *Proc. Integrated Ocean Drilling Program* 318 (Integrated Ocean Drilling Program Management International, 2011).
20. Fielding, *et al.* Facies architecture of the CRP-3 drillhole, Victoria Land Basin, Antarctica. *Terr. Antarct.* **8**, 217–224 (2001).
21. Galeotti, S. *et al.* Cyclochronology of the Eocene–Oligocene transition from a glaciomarine succession off the Victoria Land coast, Cape Roberts Project, Antarctica. *Palaeogeogr. Palaeoclimatol. Palaeoecol.* **335–336**, 84–94 (2012).
22. Barron, J. B. *et al.* *Proc. ODP Scientific Results Leg 119* (Ocean Drilling Program, 1991).
23. O'Brien, P. E. *et al.* *Proc. ODP, Init. Repts.*, 188 (Ocean Drilling Program, 2001).
24. Wilson, D. S. *et al.* Antarctic topography at the Eocene–Oligocene Boundary. *Palaeogeogr. Palaeoclimatol. Palaeoecol.* **335–336**, 24–36 (2012).
25. Escutia, *et al.* Cenozoic ice-sheet history from east Antarctic Wilkes Land continental margin sediments. *Glob. Planet. Change* **45**, 51–81 (2005).
26. Close, D. I., Watts, A. B. & Stagg, H. M. J. A marine geophysical study of the Wilkes Land rifted continental margin, Antarctica. *Geophys. J. Int.* **177**, 430–450 (2009).
27. Stickley, C. E. *et al.* Timing and nature of the deepening of the Tasmanian Gateway. *Paleoceanography* **19**, PA4027 (2004).
28. Hambrey, M. J., Ehrmann, W. U. & Larsen, B. in *Proc. Ocean Drilling Program, Scientific Results* Vol. 119 (eds Barron, J. B. *et al.*) 77–132 (Ocean Drilling Program, 1991).
29. Erohina, T. *et al.* in *Proc. ODP, Sci. Results* Vol. 188 (eds Cooper, A. K., O'Brien, P. E. & Richter, C.) 1–21 (Ocean Drilling Program, 2004).
30. Pollard, D. & DeConto, R. M. Modelling West Antarctic ice sheet growth and collapse through the past five million years. *Nature* **458**, 329–332 (2008).

Acknowledgements

This work was financially supported by the Netherlands Organization for Scientific Research (NWO, Project Number ALW-GO-A0/02-05). P.S. acknowledges financial support from the Academy Professorship awarded by the Royal Netherlands Academy of Arts and Sciences (KNAW) to H. Oerlemans. C.E. acknowledges financial support from the Spanish Ministry of Science and Education grant No. CTM2011-24079. A.J.P.H. acknowledges financial support from Statoil. S.P. acknowledges support from the National Science Foundation's Office of Polar Programs (Award Number ANT-1245283). The authors are grateful to IODP for the samples collected during Expedition 318 to Wilkes Land. This research has been sponsored by the COST Action ES0701. The authors are grateful to VPRO TV and the Beagle Series. Further support was provided by the US National Foundation under awards ANT-0424589, 1043018 and OCE-1202632.

Author contributions

P.S., C.E., H.B., B.L.A.V., A.J.P.H. and P.K.B. designed the research. P.S. and B.L.A.V. performed the GIA simulations. A.J.P.H., P.K.B., S.G., S.P. and C.E. compiled and generated field data. C.E. generated seismic stratigraphy data. R.M.D. and D.P. generated the ice-sheet model. All authors contributed to writing the paper.

Additional information

Supplementary information is available in the [online version of the paper](#). Reprints and permissions information is available online at www.nature.com/reprints. Correspondence and requests for materials should be addressed to P.S.

Competing financial interests

The authors declare no competing financial interests.

Henk Brinkhuis^{9,10}, Carlota Escutia¹¹, Adam Klaus¹², Annick Fehr¹³, Trevor Williams¹⁴, James A. P. Bendle¹⁵, Peter K. Bijl¹⁰, Steven M. Bohaty¹⁶, Stephanie A. Carr¹⁷, Robert B. Dunbar¹⁸, Jose Abel Flores¹⁹, Jhon J. Gonzalez²⁰, Travis G. Hayden²¹, Masao Iwai²², Francisco J. Jimenez-Espejo²³, Kota Katsuki²⁴, Gee Soo Kong²⁵, Robert M. McKay²⁶, Mutsumi Nakai²⁷, Matthew P. Olney²⁸, Sandra Passchier²⁹, Stephen F. Pekar^{30,31}, Jörg Pross³², Christina Riesselman³³, Ursula Röhl³⁴, Toyosaburo Sakai³⁵, Prakash Kumar Shrivastava³⁶, Catherine E. Stickley³⁷, Saiko Sugisaki³⁸, Lisa Tauxe³⁹, Shouting Tuo⁴⁰, Tina van de Flierdt⁴¹, Kevin Welsh⁴² and Masako Yamane⁴³

⁹NIOZ Royal Netherlands Institute for Sea Research, PO Box 59, 1790 AB Den Burg, Texel, The Netherlands, ¹⁰Department of Earth Sciences, Faculty of Sciences, Utrecht University, Budapestlaan 4, 3584 CD Utrecht, The Netherlands, ¹¹Instituto Andaluz de Ciencias de la Tierra, CSIC-UGR, 18100 Armilla, Spain, ¹²United States Implementing Organization, Integrated Ocean Drilling Program, Texas A&M University, 1000 Discovery Drive, College Station, Texas 77845, USA, ¹³Aachen University, Institute for Applied Geophysics and Geothermal Energy, Mathieustraße 6, D-52074 Aachen, Germany, ¹⁴Lamont-Doherty Earth Observatory of Columbia University, 61 Route 9W, Palisades, New York 10964, USA, ¹⁵School of Geographical, Earth and Environmental Sciences, Aston Webb Building, University of Birmingham, B15 2TT Edgbaston, UK, ¹⁶Ocean and Earth Science, University of Southampton, National Oceanography Centre, European Way, Southampton SO14 3ZH, UK, ¹⁷Department of Chemistry and Geochemistry, Colorado School of Mines, 1500 Illinois Street, Golden, Colorado 80401, USA, ¹⁸Environmental Earth System Science, Stanford University, Stanford, California 94305-2115, USA, ¹⁹Universidad de Salamanca, 37008 Salamanca, Spain, ²⁰Instituto Andaluz de Ciencias de la Tierra, Universidad de Granada, Campus Fuentenueva s/n, 18002 Granada, Spain, ²¹Department of Geology, Western Michigan University, 1187 Rood Hall, 1903 West Michigan Avenue, Kalamazoo, Michigan 49008, USA, ²²Department of Natural Science, Kochi University, 2-5-1 Akebono-cho, Kochi 780-8520, Japan, ²³Department of Earth and Planetary Sciences, Graduate School of Environmental Studies, Nagoya University, D2-2 (510), Furo-cho, Chikusa-ku, Nagoya 464-8601, Japan, ²⁴Marine and Core Research Center, Kochi University, B200 Monobe, Nankoku, Kochi 783-8502, Japan, ²⁵Petroleum and Marine Research Division, Korea Institute of Geoscience & Mineral Resources, 30 Gajjeong-dong, Yuseong-gu, Daejeon 305-350, Korea, ²⁶Antarctic Research Centre, Victoria University of Wellington, PO Box 600, Wellington 6140, New Zealand, ²⁷Education Department, Daito Bunka University, 1-9-1 Takashima-daira, Itabashi-ku, Tokyo 175-8571, Japan, ²⁸Department of Geology, University of South Florida, Tampa, 4202 East Fowler Avenue, SCA 528, Tampa, Florida 33620, USA, ²⁹Earth and Environmental Studies, Montclair State University, 252 Mallory Hall, 1 Normal Avenue, Montclair, New Jersey 07043, USA, ³⁰School of Earth and Environmental Sciences, Queens College, 65-30 Kissena Blvd., Flushing, New York 11367, USA, ³¹Lamont Doherty Earth Observatory of Columbia University, Palisades, New York 10964, USA, ³²Paleoenvironmental Dynamics Group, Institute of Geosciences, University of Frankfurt, Altenhoferallee 1, 60438 Frankfurt, Germany, ³³USGS, 12201 Sunrise Valley Dr, Reston, Virginia 20192-0002, USA, ³⁴MARUM-Center for Marine Environmental Sciences, University of Bremen, Leobener Strasse, 28359 Bremen, Germany, ³⁵Department of Geology, Utsunomiya University, 350 Mine-Machi, Utsunomiya 321-8505, Japan, ³⁶Polar Studies Division, Geological Survey of India, NH 5P, NIT, Faridabad 121001, India, ³⁷Department of Geology, University of Tromsø, N-9037 Tromsø, Norway, ³⁸Department of Earth and Planetary Science, University of Tokyo, Science Building No. 1, room 852, 7-3-1 Hongo, Bunkyo-ku, Tokyo 113-0033, Japan, ³⁹Geosciences Research Division, Scripps Institution of Oceanography University of California, San Diego, LaJolla, California 92093-0220, USA, ⁴⁰State Key Laboratory of Marine Geology, Tongji University, 1239 Siping Road, Shanghai 200092, China, ⁴¹Department of Earth Science and Engineering, Imperial College London, South Kensington Campus, Exhibition Road, SW7 2AZ London, UK, ⁴²School of Earth Sciences, University of Queensland, St Lucia, Brisbane QLD 4072, Australia, ⁴³Earth and Planetary Science, University of Tokyo, 7-3-1 Hongo, Bunkyo-ku, Tokyo 113-0033, Japan.